Available online at www.sciencedirect.com
ScienceDirect
Nuclear Instruments and Methods in Physics Research B 255 (2007) 247–252
NIM B
Beam Interactions with Materials & Atoms
www.elsevier.com/locate/nimb

Ranges and fragmentation behavior of fullerene molecules: A molecular-dynamics study of the dependence on impact energy and target material

Christian Anders [a], H. Kirihata [b], Y. Yamaguchi [b], Herbert M. Urbassek [a,*]

[a] *Fachbereich Physik, Universität Kaiserslautern, P.O. Box 3049, Erwin-Schrödinger-Straße, D-67663 Kaiserslautern, Germany*
[b] *Department of Mechanical Engineering, Osaka University, Japan*

Available online 8 January 2007

Abstract

Using molecular-dynamics simulation, we study the impact of C_{60} fullerene molecules with energies up to several tens of keV on various target materials: graphite, fullerite, Au and a condensed Ar solid. The analysis is based on single impact events. For all the target materials, fragmentation of the fullerene projectile sets in at around 1 keV impact energy; it starts the earliest in the heavy Au target. Full atomization of the projectile is observed at around 10 keV impact energy.

The projectile ranges, on the other hand, depend strongly on the target material. The highest ranges are achieved in the weakly bonded Ar target. Also ranges in the fcc-C_{60} solid are systematically larger than in the graphite target. Interestingly, at energies above 5 keV, the fullerene penetrates deeper into the Au target than into graphite, even though the Au has a considerably higher mass and efficiently reflects the fullerenes at lower bombarding energies; this indicates the dominant role of the cohesive energy of the target.

The energy dependence of fullerene molecules is surprisingly flat and varies between $E^{1/3}$ and $E^{2/3}$ at smaller impact energies, $E < 10$ keV. At higher impact energies, where the projectile has been fully atomized, the energy dependence becomes more pronounced, $\propto E$.

PACS: 79.20.Rf; 79.20.Ap; 61.80.Lj

Keywords: Fullerene; Molecular-dynamics simulation; Cluster–surface interaction; Range

1. Introduction

The interaction of clusters and molecules with surfaces has received increased attention in recent years both due to fundamental interests and various existing or anticipated applications. Among the latter we note thin-film deposition [1,2], secondary ion (and neutral) mass spectroscopy [3] and as a desorption method for bio-molecules [4]. As a basis for an understanding of the processes occurring, the stopping of the cluster, its fragmentation and its range need to be known.

Fullerene impact on materials has been investigated using molecular-dynamics computer simulation previously. Here, the pioneering work of Webb et al. [5] on C_{60} ranges in graphite and its comparison to experimental data obtained by an oxidation technique needs be mentioned as well as the investigation of energetic C_{60} impact and thin-film growth on a Si surface by Smith and Beardmore [6]. Further work on fullerene bombardment focused on the induced sputtering [7]. More recently, Postawa et al. [8] compared the consequences of a C_{60} cluster impact and a Ga atom impact, each with 15 keV (total) energy, on Ag (111); they demonstrated that C_{60} projectiles are eminently efficient in producing sputtering. The same group recently published further simulations on various aspects of C_{60} impact on elemental surfaces [9–11], but also

* Corresponding author. Tel.: +49 6312053022; fax: +49 6312053907.
E-mail address: urbassek@rhrk.uni-kl.de (H.M. Urbassek).
URL: http://www.physik.uni-kl.de/urbassek/ (H.M. Urbassek).

0168-583X/$ - see front matter © 2006 Elsevier B.V. All rights reserved.
doi:10.1016/j.nimb.2006.11.027

on frozen H_2O surfaces [13,12] and on thin overlayer films [14,15]. Ion bombardment of fullerite films has also been studied by simulation quite early; thus, Hobday et al. [16] focused on sputtering, but also reported on the damage induced in the film.

In the present paper, we wish to extend these previous studies and investigate the fragmentation behavior and range of fullerene molecules in matter. For this purpose, impact energies are chosen, which span the regime of intact stopping (or reflection) to that of complete atomization of the projectile. Four different target materials are chosen, which vary greatly in their cohesion and their mass: graphite, fullerite, condensed Ar and Au.

2. Systems

A fullerene (C_{60}) molecule forms the projectile. It impinges with a total energy E, which varies between 0.1 and 80 keV, on the following materials:

1. A graphite crystal with a (0 0 0 1) surface. For impact energies below 24 keV, our crystallite consists of 63,000 atoms; it has a depth of 120 Å (37 layers) and a lateral extension of 68 Å. For impact energies above 24 keV, the crystal depth has been increased to 150 Å, and at 80 keV to 214 Å.
2. A fullerite crystal. This fcc crystal has a (1 1 1) surface. It consists of 1708 C_{60} molecules organized in a hexagonal conical shape. The lateral extension at the surface is 163 Å, the maximum depth of the crystallite is 81 Å. The outermost layers of this crystallite are controlled by a Langevin thermostat, which keeps the vibrational and translational temperature in this region at 200 K; the heat exchange rate corresponds to the thermal conductivity of fullerite.
3. A Au crystal with a (1 0 0) surface. It consists of 37,000 atoms organized in a cubic shape with a side length of 84 Å. In contrast to the other target materials, this crystallite had an initial temperature of 300 K in order to prevent the channeling of C atoms, which was observed at 0 K.
4. An amorphous Ar target. Here, 148,201 atoms are employed, which are organized in a volume with a lateral extension of 100 Å and a depth of 540 Å.

All targets employed damped boundaries at the bottom and lateral sides [17,18]. The simulation time varied between 1 and 12 ps, depending primarily on the target material, but also on the impact energy. In each case we made sure that the projectile – or its fragments – had reached its maximum depth inside the target material before the simulation was stopped. Note that the simulation volume is smaller than that employed for sputtering or damage simulations, in which the time dependence of the energy dissipation – and hence the target size – may be critical in controlling the sputtering and damage yields; since cluster *ranges* are determined on a smaller time scale, we are confident that our results on ranges are reliable. For each bombarding energy and target material only a single impact event was simulated, since we assume that the range straggling for the large clusters considered here is small. Possibly, impact on fullerite forms an exception, since at low energies, where the projectile is not destroyed, the exact location of the impact point may be relevant; but also in this case, at higher energies, this dependence will disappear upon disintegration of the projectile. In our study, we chose a central head-on collision geometry between the impacting fullerene molecule and a target molecule.

For the C–C interaction, two different interaction potentials were employed: A bond-order potential [19] where special care was taken to describe the weak interlayer attraction of the graphite basal planes, was employed in particular to describe the graphitic target appropriately [20]. For the fullerite crystal, on the other hand, the short-range bond-order potential by Brenner [21] was used besides a long-range Lennard–Jones potential [22] with parameters $\sigma = 3.37$ Å, $\epsilon = 2.40$ meV connected via a switching function. The fullerene projectile is well described by either of these two potential forms. For the Au crystal, a Au–Au interaction potential of a many-body form was chosen [23], while Ar is well described by the Lennard–Jones potential [24–26]. The interspecies potentials were based on pair potentials: For the C–Ar interaction, a Lennard–Jones potential with parameters $\sigma = 3.385$ Å, $\epsilon = 5.001$ meV was chosen [27], while the C–Au potential was described by a Morse potential with parameters $D = 0.153$ eV, $r_e = 2.6$ Å, $\beta = 2.6$ Å^{-1} [28]. All the inter- and intra-species potentials were extrapolated to an appropriate high-energy interaction potential [29,30].

3. Results

Fig. 1 displays cross-sectional views of the various materials that were bombarded by a fullerene molecule. An impact energy of 6 keV was chosen, which represents the case of almost complete fragmentation of the projectile. Among the different target materials chosen, we first discuss the two polytypes of carbon, viz. graphite and fullerite; these materials have the same atomic mass as the projectile, but differ largely in their bonding properties. While the (0 0 0 1) planes of graphite are internally strongly bonded, the interplanar bonding is mediated by the π-electronic system and is relatively weak. In contrast to the planar structure of graphite, fullerene molecules form the basic building blocks of fullerite; their strong internal bonding is contrasted by a weak van-der-Waals-like intermolecular interaction. Fig. 1(a) and (b) shows that the fullerene molecule impact creates a temporary crater in the target. In graphite, the planar structure has been destroyed at the bottom of the crater and projectile atoms have been mixed with target atoms in this region, forming an amorphous C layer. Due to the projectile momentum and the excess density at the crater bottom, the intact graphite planes below the crater have temporarily become curved

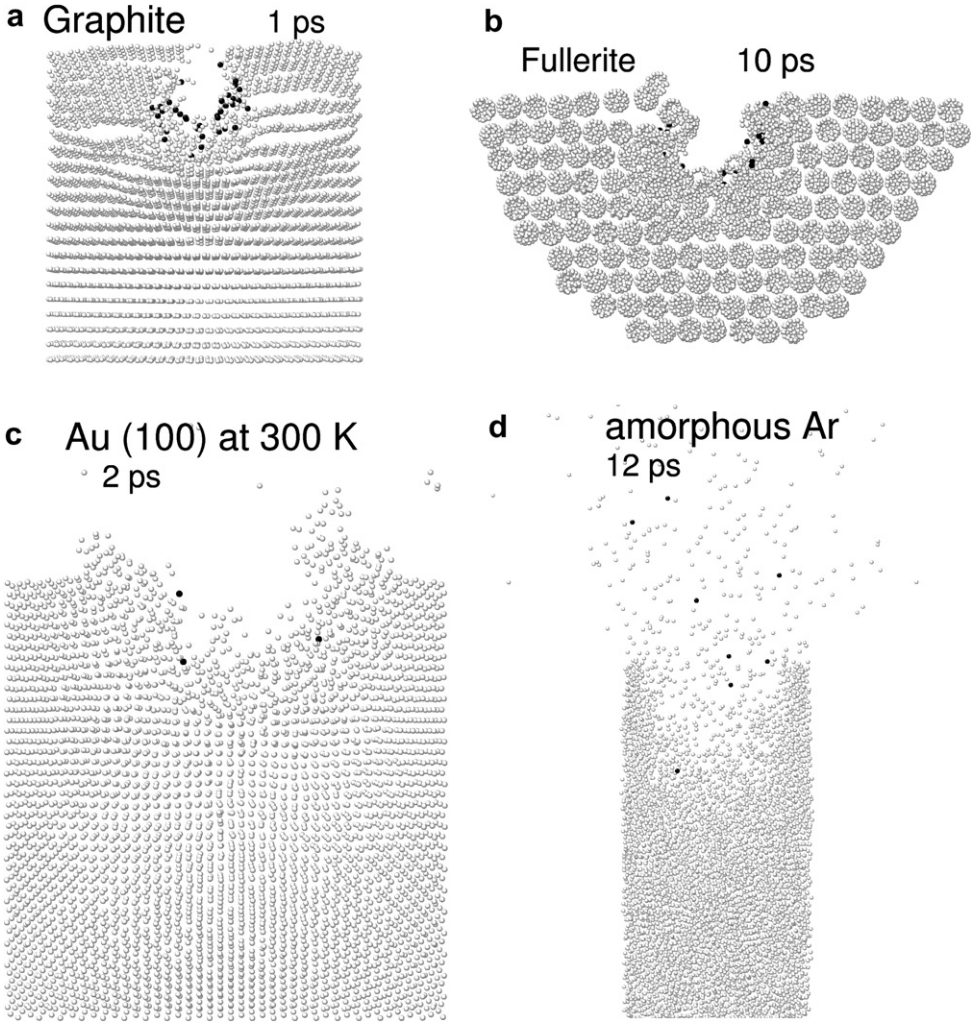

Fig. 1. Cross-sectional view (thickness 10 Å, lateral size d of simulation volume varies as indicated below) through several materials penetrated by fullerene molecules with an impact energy of $E = 6$ keV. The times t after impact (indicated in the figures) have been chosen such that the projectile reached its deepest position then. Dark: projectile atoms, light: target atoms. (a) Graphite, $d = 68$ Å. (b) Fullerite, impact energy $E = 5$ keV, displayed lateral size 145 Å. (c) Au, $d = 84$ Å. (d) Amorphous Ar, $d = 100$ Å.

towards the target inner. Similarly, in fullerite besides the crater formed, the target fullerene molecules at the bottom and the sidewalls of the crater have been destroyed and the projectile atoms have been mixed into the amorphous carbon formed there. The fullerene atomic planes below the crater have been better conserved, due to their high stopping efficiency. Cross-linking of C_{60} molecules and the onset of polymerization can be observed [16]. Note that the crater in the two carbon materials, graphite and fullerite, is not of a hemispherical shape, but rather of a pear-like form, in which the lower part of the crater has a wider radius than the constrained upper neck. This is in contrast to the case of metals, which show a hemispherical crater shape at comparative bombarding conditions. We presume that this pear-like shape is due to the special nature of the C_{60} projectile, which passes the first distance in the target in a relatively compact form and only fragments and 'explodes' deeper inside the material, creating the extended bottom part of the crater.

The crater created in Au, illustrated in Fig. 1(c), is considerably shallower than that created in the carbon materials. This is due to the large ratio of target to projectile atom mass which leads to an efficient stopping of the projectile. Note that the hemispherical crater form is accompanied by the formation of crater rims, from which the sputtering of atoms can still be observed. This crater form is typical of cluster-induced craters in metallic targets [31]. The metallic target is only little compressed at the crater bottom; rather the target material flows sideways out of the crater towards the surface and thus forms the crater rims observed.

Finally, the bombardment of an amorphous Ar target shown in Fig. 1(d) exemplifies the effect of a small cohesive target energy. Here, projectile atoms penetrate deeper into the material than in the cases discussed previously. Even more spectacular is the different crater formation mechanism, which operates in this case via evaporation of the target material. Here the energy input is so large that a large part of the near-surface material in the vicinity of

the impact boils away due to the small target binding energy. The process is evidently not yet finished at the moment when this plot has been taken. At later times, the projectile atoms will be entrained in the gas flow of the evaporating target atoms and leave the material.

In Fig. 2, we quantify the ranges of fullerene molecules in the materials studied. Two different range measures have been chosen. R_{max} denotes the maximum depth which a projectile atom achieves in the simulation. For its determination, we monitored the time dependence of the positions of all carbon atoms of the fullerene projectile and determined its maximum. As a further measure, we monitored the mean range R_{cm} as the maximum depth of the center of mass defined by all the projectile atoms. For small impact energies the center of mass may remain above the surface, yielding nominally *negative* range values; therefore, in the presentation of Fig. 2(b) we plot $R_{cm} + r$ with $r = 3.64$ Å as the radius of a fullerene molecule.

Fig. 2(a) shows that throughout the energy range studied for fullerite, $E < 10$ keV, the ranges in graphite are consistently smaller than those in fullerite. This can be attributed to the strong bonding within the graphite planes, which efficiently stops the projectile and leads to smaller ranges. Note, however, that the energy dependence of the ranges in the two carbon polytypes is rather different; while the fullerite data exhibit a shallow energy dependence, $\propto E^{1/3}$, the graphite ranges are steeper, $\propto E^{2/3}$, up to an impact energy of 10 keV. Beyond this energy a steeper dependence, $\propto E$, is found.

Not surprisingly, the ranges in Au are extremely small for energies $E \leqslant 1$ keV. Here the fullerene molecules are effectively reflected off the Au surface. At energies above around 5 keV, the penetration depths are comparable to those in graphite. This may appear astonishing, in view of the large mass mismatch between Au and carbon atoms. However, for these energies, the fullerene molecules almost completely fragment, and the fragment carbon atoms have only a small stopping cross-section in Au.

Finally, fullerene projectiles can penetrate to a considerable depth in Ar. At 10 keV impact energy we find maximum ranges of around 100 Å and mean ranges of 60 Å. This material exemplifies the role of the target cohesive energy on projectile stopping.

Interestingly, the ranges show a non-monotonic dependence on the impact energy. This is most clearly seen for the mean range in the condensed Ar target, Fig. 2(b), but

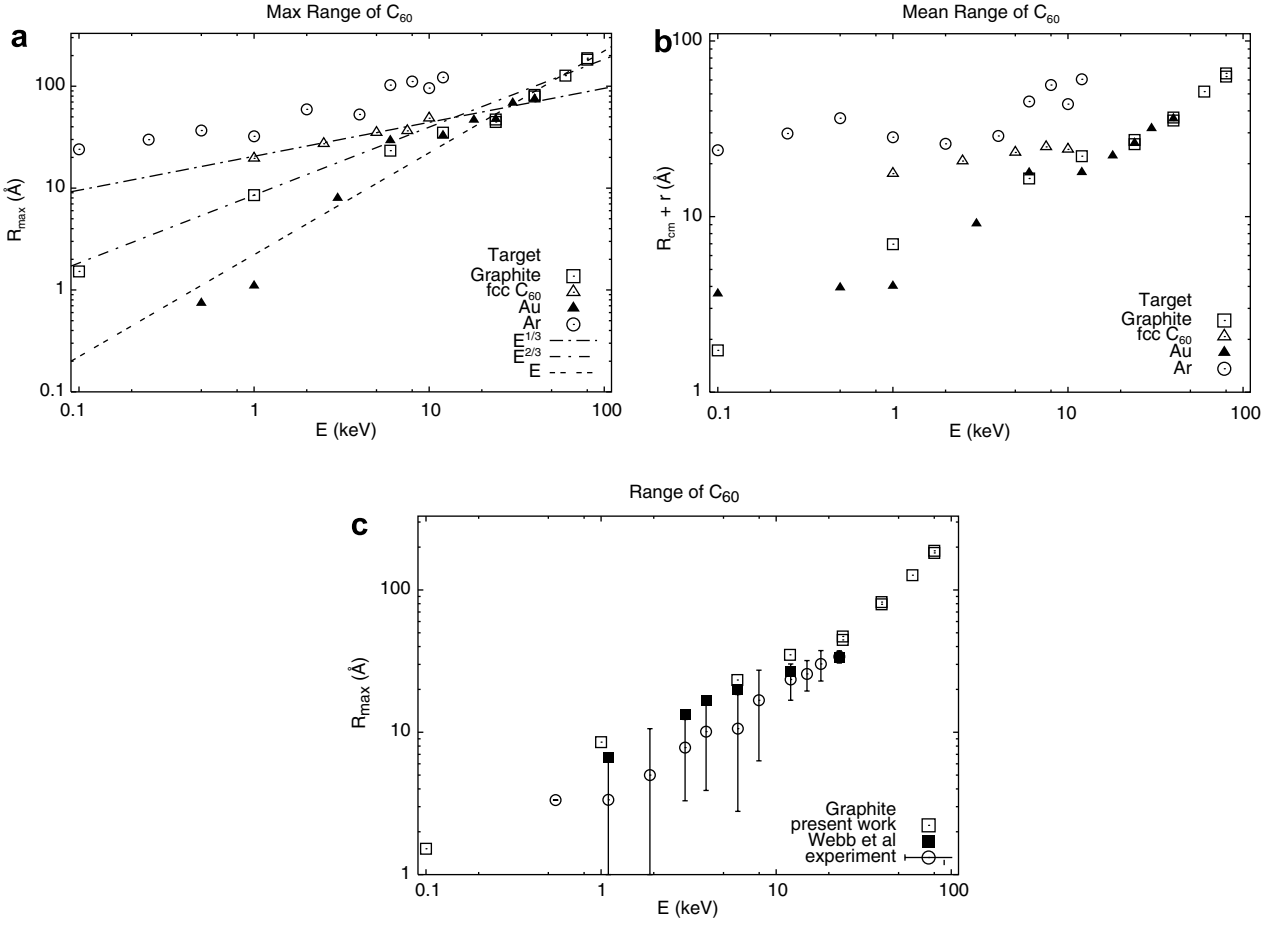

Fig. 2. Energy dependence of the range of fullerene molecules in various materials. (a) Maximum range R_{max}. Lines showing polynomial energy dependences have been added for comparison. (b) Mean range. Here, we plot $R_{cm} + r$ where $r = 3.64$ Å is the radius of a fullerene molecule. (c) Comparison of experimental and previous simulational data (both taken from [5]) of $C_{60} \rightarrow$ graphite impact to our R_{max} ranges.

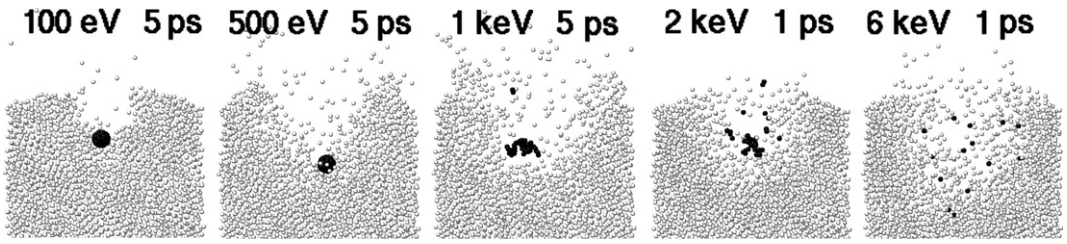

Fig. 3. Cross-sectional view (cf. Fig. 1) of an amorphous Ar sample impacted by fullerene molecules of various energies.

also in the other data. This behavior is connected to the fragmentation of the fullerene projectile: when fragmentation sets in, the mean range decreases and only starts increasing again at higher impact energies. This dependence demonstrates the increased range of clusters with respect to equi-velocity atoms.

We note that Webb et al. [5] studied the energy dependence of fullerene ranges in graphite. They identified the range as the deepest graphite layer which was left unbroken by the impact. As Fig. 2(c) shows, their ranges are similar to ours and in close agreement to the experimental data reported in the same reference.

Fig. 3 visualizes the fragmentation of fullerene molecules upon impact onto an amorphous Ar sample. While at energies of 100 and 500 eV, the molecule is embedded intact into the Ar sample, it strongly deforms at 1 keV, fragments at 2 keV and atomizes at 6 keV impact energy.

Fig. 4 quantifies the energy dependence of the fragmentation of fullerene molecules upon impact on the various materials studied. As a characteristic quantity describing the fragmentation behavior we chose the number of fragments formed. This quantity assumes values between 1 for the intact molecule and 60 for the fully atomized projectile. In agreement with the high intra-molecular bonding of the fullerene molecule, we find virtually no fragmentation for impact energies below 0.5–1 keV. On the other hand, above $E \gtrsim 10$ keV, the projectile completely fragments.

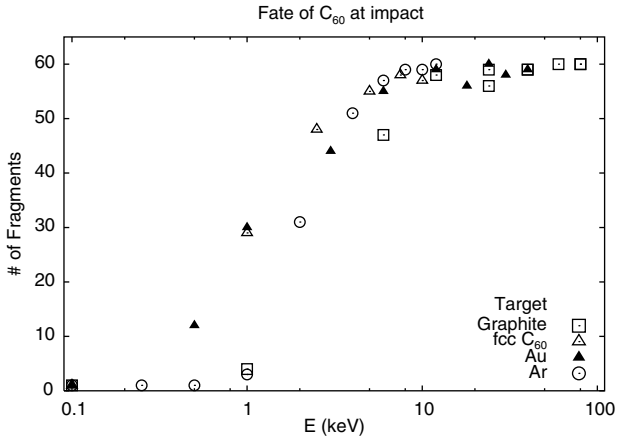

Fig. 4. Energy dependence of the number of projectile fragments generated by the impact of fullerene molecules on various materials.

In the intermediate energy regime, $1\text{ keV} \leqslant E \leqslant 10\text{ keV}$, the fragmentation behavior depends on the target material. Thus Au leads to strong fragmentation; this behavior can be rationalized by the high Au atom mass. In contrast, impact upon graphite leads to the smallest fragmentation, while fullerite and Ar are located at intermediate places.

4. Conclusions

Using molecular-dynamics computer simulation, we studied the range and fragmentation behavior of C_{60} molecules in various target materials. The analysis is based on single impact events.

1. The range of fullerene molecules in the two carbon polytypes studied (graphite and fullerite) was found to be not only quantitatively different, but also to follow different energy dependences. This demonstrates the strong influence of the target atom bonding on the projectile ranges.
2. Ranges in Au were the smallest of those studied. This can be attributed to the large atomic mass mismatch between the projectile and target atoms.
3. Fullerene molecules could penetrate deepest into the weakly bound Ar target, again exemplifying the role of target atom bonding.
4. Below around 500 eV impact energy, fullerene molecules stayed intact, while above 5–10 keV, they completely disintegrated for all the target materials studied. In the intermediate energy range, fragmentation sets in most strongly in Au (due to the pronounced mass mismatch) and in fullerite (due to the set-in of polymerization reactions).
5. As soon as the projectile starts to fragment, the projectile range ceases to increase and may even decrease somewhat with increasing projectile energy. This behavior exemplifies the increased range of clusters with respect to equi-velocity atoms.

Acknowledgement

H. Kirihata appreciates the support from the Uomoto International Scholarship Foundation for the student exchange system.

References

[1] W.L. Brown, M.F. Jarrold, R.L. McEachern, M. Sosnowski, G. Takaoka, H. Usui, I. Yamada, Nucl. Instr. and Meth. B 59/60 (1991) 182.
[2] H. Haberland, Z. Insepov, M. Moseler, Z. Phys. D 26 (1993) 229.
[3] J.C. Vickerman, D. Briggs (Eds.), ToF-SIMS: Surface Analysis by Mass Spectrometry, IM Publications, Chichester, UK, 2001.
[4] A. Tempez, J.A. Schultz, S. Della-Negra, J. Depauw, D. Jacquet, A. Novikov, Y. LeBeyec, M. Pautrat, M. Caroff, M. Ugarov, et al., Rapid Commun. Mass Spectrom. 18 (2004) 371.
[5] R.P. Webb, M. Kerford, M. Kappes, G. Brauchle, Radiat. Eff. Defects Solids 142 (1997) 23.
[6] R. Smith, K. Beardmore, Thin Solid Films 272 (1996) 255.
[7] R. Smith, K. Beardmore, A. Gras-Marti, R. Kirchner, R.P. Webb, Nucl. Instr. and Meth. B 102 (1995) 211.
[8] Z. Postawa, B. Czerwinski, M. Szewczyk, E.J. Smiley, N. Winograd, B.J. Garrison, Anal. Chem. 75 (2003) 4402.
[9] Z. Postawa, B. Czerwinski, M. Szewczyk, E.J. Smiley, N. Winograd, B.J. Garrison, J. Phys. Chem. B 108 (2004) 7831.
[10] S. Sun, C. Szakal, E.J. Smiley, Z. Postawa, A. Wucher, B.J. Garrison, N. Winograd, Appl. Surf. Sci. 231–232 (2004) 64.
[11] K.D. Krantzman, D.B. Kingsley, B.J. Garrison, Appl. Surf. Sci. 252 (2006) 6463.
[12] I.A. Wojciechowski, B.J. Garrison, J. Phys. Chem. A 110 (2006) 1389.
[13] M.F. Russo Jr., I.A. Wojciechowski, B.J. Garrison, Appl. Surf. Sci. 252 (2006) 6423.
[14] Z. Postawa, B. Czerwinski, N. Winograd, B.J. Garrison, J. Phys. Chem. B 109 (2005) 11973.
[15] B. Czerwinski, A. Delcorte, B.J. Garrison, R. Samson, N. Winograd, Z. Postawa, Appl. Surf. Sci. 252 (2006) 6419.
[16] S. Hobday, R. Smith, U. Gibson, A. Richter, Radiat. Eff. Defects Solids 142 (1997) 301.
[17] J.R. Beeler Jr., Radiation Effects Computer Experiments, North-Holland, Amsterdam, 1983.
[18] H. Gades, H.M. Urbassek, Phys. Rev. B 51 (1995) 14559.
[19] K. Nordlund, J. Keinonen, T. Mattila, Phys. Rev. Lett. 77 (1996) 699.
[20] M. Henkel, H.M. Urbassek, Nucl. Instr. and Meth. B 145 (1998) 503.
[21] D.W. Brenner, Phys. Rev. B 42 (1990) 9458 (Erratum: Phys. Rev. B 46 (1992) 1948).
[22] S. Maruyama, T. Kimura, Proc. ASME Heat Transfer Div. 2 (2000) 405.
[23] T.J. Colla, H.M. Urbassek, Nucl. Instr. and Meth. B 164–165 (2000) 687.
[24] A. Michels, H. Wijker, H.K. Wijker, Physica 15 (1949) 627.
[25] J.-P. Hansen, L. Verlet, Phys. Rev. 184 (1969) 151.
[26] C. Anders, H.M. Urbassek, R.E. Johnson, Phys. Rev. B 70 (2004) 155404.
[27] Y. Yamaguchi, J. Gspann, Phys. Rev. B 66 (2002) 155408.
[28] R. Smith, C. Nock, S. Kenny, J.J. Belbruno, M. Di Vece, S. Palomba, R.E. Palmer, Phys. Rev. B 73 (2006) 125429.
[29] W.D. Wilson, L.G. Haggmark, J.P. Biersack, Phys. Rev. B 15 (1977) 2458.
[30] J.F. Ziegler, J.P. Biersack, U. Littmark, The Stopping and Range of Ions in Solids, Pergamon, New York, 1985.
[31] R. Aderjan, H.M. Urbassek, Nucl. Instr. and Meth. B 164–165 (2000) 697.